A Dust-penetrated Classification Scheme for Bars as Inferred from Their Gravitational Force Fields

R. Buta – University of Alabama

D. L. Block – University of the Witwatersand

Citation of published version:

Buta, R., Block, D. (2001): A Dust-penetrated Classification Scheme for Bars as Inferred from Their Gravitational Force Fields. *The Astrophysical Journal,* 550(1).
DOI: 10.1086/319736

The Astrophysical Journal, 550:243–252, 2001 March 20

A DUST-PENETRATED CLASSIFICATION SCHEME FOR BARS AS INFERRED FROM THEIR GRAVITATIONAL FORCE FIELDS

R. Buta[1] and D. L. Block
Department of Computational and Applied Mathematics, University of the Witwatersrand, Private Bag 3, WITS 2050, South Africa
Received 2000 August 10; accepted 2000 November 9

ABSTRACT

The division of galaxies into "barred" (SB) and "normal" (S) spirals is a fundamental aspect of the Hubble galaxy classification system. This "tuning fork" view was revised by de Vaucouleurs, whose classification volume recognized apparent "bar strength" (SA, SAB, SB) as a continuous property of galaxies called the "family." However, the SA, SAB, and SB families are purely visual judgments that can have little bearing on the actual bar strength in a given galaxy. Until very recently, published bar judgments were based exclusively on blue light images, where internal extinction or star formation can either mask a bar completely or give the false impression of a bar in a nonbarred galaxy. Near-infrared camera arrays, which principally trace the old stellar population in both normal and barred galaxies, now facilitate a quantification of bar strength in terms of their gravitational potentials and force fields. In this paper, we show that the maximum value, Q_b, of the ratio of the tangential force to the mean axisymmetric radial force in a barred disk galaxy is a quantitative measure of the strength of a bar. Q_b does not measure bar ellipticity or bar shape but rather depends on the actual forcing due to the bar embedded in its disk. We show that a wide range of true bar strengths characterizes the category "SB," while the de Vaucouleurs category "SAB" corresponds to a narrower range of bar strengths. We present Q_b values for 36 galaxies, and we incorporate our bar classes into a dust-penetrated classification system for spiral galaxies.

Subject heading: galaxies: kinematics and dynamics — galaxies: spiral — galaxies: structure

1. INTRODUCTION

The presence of a bar in a disk galaxy implies a nonaxisymmetric gravitational field. The high frequency of occurrence of bars (over 65%; de Vaucouleurs 1963; Eskridge et al. 2000) and the fact that bars principally consist of an old stellar population (de Vaucouleurs 1955; de Vaucouleurs & de Vaucouleurs 1959; Freeman 1989; Elmegreen & Elmegreen 1985) implies that bars are fundamental components in the distribution of mass in galaxies.

Bars are believed to be the "engines" driving a wide variety of secular evolution processes in galaxy dynamics (Pfenniger, Martinet, & Combes 1996). Bar-driven secular evolution appears to make significant changes in galaxy structure over a Hubble time. The main components found in barred galaxies include bulges, disks, lenses, and inner and outer rings—and of course the bar itself (Sandage 1961; de Vaucouleurs 1959; Kormendy 1979; Sellwood & Wilkinson 1993; Buta 1995; Buta & Combes 1996).

The absence or presence of a bar led Hubble (1926) to develop two separate prongs to his classification "tuning fork": the sequence of normal (unbarred) spirals Sa, Sb, and Sc, paralleled by a sequence of barred spirals SBa, SBb, and SBc. De Vaucouleurs (1959) recognized that galaxies such as NGC 5236 (M83) showed a bar morphology intermediate between that of a normal and a barred spiral. He introduced the notation SA for unbarred spirals so that he could use the combined notation SAB for transitional cases like M83.

In this paper, we recognize a full continuum of "bar strengths," as does de Vaucouleurs, but we propose a numerical quantification of bar strength based on the gravitational forcing of the bar itself, not on visual appearance. From a sample of 36 galaxies, we recognize seven bar strength classes: bar class 0 galaxies, which are normal spiral galaxies without any bar; bar class 1 and 2 galaxies, which show ovals and weak bars (which de Vaucouleurs would have classified in his SAB class); and bar class 2–6 galaxies, which encompass all galaxies classified as SB by Hubble and de Vaucouleurs.

Our numerical quantification of bar strength is derived from the nonaxisymmetric force field of a galaxy inferred from the near-infrared light distribution. Near-infrared H-band (effective wavelength 1.6 μm) and K-band (effective wavelength 2.2 μm) images beautifully reveal the old stellar population or "backbone" of spiral galaxies (Frogel, Quillen, & Pogge 1996; Block et al. 1994; Block et al. 1999). The near-infrared light comes principally from old giant and supergiant stars (Frogel et al. 1996). The extinction at H and K is only 0.1–0.2 times that in visual light, so that dust has only a minimal effect on the inferred potentials. A rich duality of spiral structure has been found from studies of optical and near-infrared images; a spiral galaxy may present two completely different morphologies when examined optically and in the near-infrared (Elmegreen et al. 1999; Block et al. 1999).

In the optical, dust often hides bars, as in the Milky Way. Seventy percent of spirals classified in the Carnegie Atlas of Galaxies (Sandage & Bedke 1994), based on Hubble bins, are classified as unbarred. This fraction drops to 27% when these galaxies are imaged in the near-infrared (Eskridge &

[1] Permanent address: Department of Physics and Astronomy, University of Alabama, Box 870324, Tuscaloosa, Alabama 35487.

Frogel 1999). The remaining 43% show ovals or bars in the dust-penetrated regime. This high percentage of bars in the near-infrared agrees with the findings of Seigar & James (1998), who found that 90% of a sample of 45 galaxies showed some evidence of a bar in the K band.

2. BAR STRENGTH AS A MEASURABLE PARAMETER OF GALAXIES

A variety of quantitative parameters has been suggested or could be interpreted to represent a measure of the "strength" of a bar. The bar-interbar contrast, developed by Elmegreen & Elmegreen (1985), can distinguish strong bars from weak bars but may connect only indirectly to an actual bar strength. Sometimes the maximum bar-interbar contrast occurs inside the radius of the bar, but in some cases it may occur outside the ends of the bar, as in NGC 1433 (Buta 1986). Also, Seigar & James (1998) note that bar-interbar contrasts may be weakened by resolution and seeing effects.

Elmegreen & Elmegreen (1985) also used Fourier intensity amplitudes to derive relative bar luminosities in terms of $m = 2$ and 4 components. Relative to the total luminosity of the disk within the standard isophote having $\mu_B = 25.0$ mag arcsec^{-2}, the bar luminosity fraction was found to range from less than 1% to more than 20%. Ohta, Masau, & Wakamatsu (1990) derive similar parameters for six barred galaxies, including the $m = 6$ term.

The most popular bar strength parameter, because of its simplicity, is the deprojected bar ellipticity, ϵ_b, developed by Martin (1995) and suggested by analytical models (Athanassoula 1992) to be a readily accessible measure of the strengths of bars that does not depend on spectroscopic observations, surface photometry, or mass-to-light ratio assumptions. Martin (1995) derived ϵ_b for more than 100 spiral galaxies by visual inspection of published optical photographs and noted that the slope of chemical abundance gradients (Martin & Roy 1994) as well as the presence of nuclear star formation (Martin & Friedli 1997) depend on ϵ_b. This parameter [or its equivalent, $(b/a)_{\rm bar}$] has also been used in a number of other recent papers (Rozas, Knapen, & Beckman 1998; Aguerri 1999; Chapelon, Contini, & Davoust 1999; Abraham et al. 1999; Shlosman, Peletier, & Knapen 2000). Abraham et al. (1999) describe an algorithm that automatically derives $(b/a)_{\rm bar}$ from moments of the galaxy image taken at various cuts relative to the maximum flux level. This approach is useful for high-redshift morphological studies. Abraham & Merrifield (2000) describe a refinement on bar axis ratio using a parameter $f_{\rm bar}$, defined as "the minimum fraction of the bar's stars that one would have to rearrange in order to transform the structure into an axisymmetric distribution." Martin (1995) notes that ϵ_b is not a complete description of bar strength but merely the most accessible one.

Seigar & James (1998) developed another quantitative approach to bar strength that utilized near-infrared surface photometry. In their method, the bar is defined to be the light remaining after disk and bulge components are subtracted. This light is converted into a parameter known as "equivalent angle," which is defined to be "the angle subtended at the centre of the galaxy by a sector of the underlying disk and bulge that emits as much light as the bar component, within the same radial limits." An advantage of this method is that it accounts for both conventional bars as well as ovals. However, the method relies on full bulge/disk photometric decompositions, which can be very difficult for strongly barred galaxies. Rozas et al. (1998) derived another flux parameter, σ_b, representing the ratio of the flux inside the bar to that outside the bar area. They argue that this parameter and ϵ_b indicate that stronger bars are accompanied by a lower degree of symmetry of star formation in the spiral arms.

In each of these methods, the bar itself has to be defined, e.g., where it appears to start, where it appears to end, or where the maximum ellipticity is achieved. Our approach here is different and is based instead on the torques induced by the rigidly rotating bar, without first having to accurately define and isolate it relative to the other components in a galaxy.

3. BAR STRENGTH AS A FORCE RATIO RATHER THAN AN AXIS RATIO

The most elegant way of measuring the torques of bars embedded in disks is actually an old idea. Given the gravitational potential $\Phi(R, \theta)$ in the disk plane, Combes & Sanders (1981) proposed defining the bar strength at radius R as

$$Q_T(R) = \frac{F_T^{\max}(R)}{\langle F_R(R) \rangle}, \quad (1)$$

where $F_T^{\max}(R) = [\partial\Phi(R, \theta)/\partial\theta]_{\max}$ represents the maximum amplitude of the tangential force at radius R and $\langle F_R(R) \rangle = R(d\Phi_0/dR)$ is the mean axisymmetric radial force at the same radius, derived from the $m = 0$ component of the gravitational potential. Although Q_T depends on radius, the maximum value of Q_T can provide a single measure of bar strength for a whole galaxy, if the gravitational potential is known. With the advent of near-infrared arrays and the availability of many high quality K- and H-band images of galaxies covering a range of apparent bar morphologies, it has become possible for the first time to use the idea in equation (1) in a practical way to directly measure the strengths of bars from their force fields for a large number of galaxies. This provides us with an opportunity to develop a consistent and robust scheme of dust-penetrated classification of bars embedded within disks. We outline our application of equation (1) here in a preliminary way using a small sample of near-infrared images and discuss its advantages and disadvantages over the methods just described. Our subset of near-infrared images comes mainly from a much larger sample used to develop a near-infrared classification scheme of spiral galaxies, based on a wide variety of telescopes and detectors. Except for Maffei 2 and M101, full details of the observing procedures, integration times, filters, and image scales have been described and published in Block et al. (1994), Block et al. (1999), and references therein. The images of Maffei 2 and M101 that we have used are from the Two Micron All-Sky Survey (Jarrett 2000) and have an image scale of 1″ pixel^{-1}.

4. GRAVITATIONAL POTENTIALS OF GALAXIES FROM NEAR-INFRARED IMAGES

Quillen (1996) reviews the principal issues in deriving gravitational potentials from near-infrared images. The principal assumption is that the light traces the mass; i.e., the mass-to-light ratio is constant across much of the disk. Then the potential in two dimensions can be derived as the convolution of the mass density with the function $1/R$ using fast Fourier transform techniques (Binney & Tremaine 1987, p. 90).

The validity of the constant M/L assumption can be evaluated from detailed rotation curve studies or from multicolor near-infrared surface photometry. For example, Freeman (1992) reported an analysis of a sample of more than 550 Hα rotation curves and I-band surface photometric profiles derived by Mathewson, Ford, & Buchhorn (1992), which shows that the stellar mass distribution alone, with $M/L \sim$ constant, reproduces the observed optical rotation curves for about 97% of their sample. The rotation curve morphologies cited by Freeman span the entire range: from almost entirely solid body to almost entirely flat. In a more recent study, Persic, Salucci, & Stel (1996) corroborate this result and show that the optical rotation curves of spiral galaxies may be fitted by a constant mass-to-light ratio (except for dwarf galaxies, none of which we study here).

Constraints on the dark halo content of barred galaxies may also be deduced from the dynamical friction or drag of bars rotating within dark matter halos. The studies of Debattista & Sellwood (1998, 2000) indicate that bars are able to maintain their high pattern speeds only if the disk itself provides most of the gravitational potential—a high central density, dark matter halo would simply provide too much drag on the bar. Such independent studies suggest that light effectively traces mass within the optical disks of barred spiral galaxies. A detailed dynamical study of one barred spiral, NGC 4123, by Weiner (1998) shows that the inner regions of the disk must be at 90%–100% of the required "maximum disk" forcing.

The method and program that we will use to derive potentials for our sample galaxies is described by Quillen, Frogel, & González (1994), hereafter QFG. These authors describe a practical application of the convolution equations that can be used on two-dimensional images and that explicitly accounts for disk thickness. By assuming that the z-dependence of the mass density is independent of position in the plane, the potential can be derived as the convolution of the image intensities with a function that integrates over the vertical dependence of the density, $\rho_z(z)$. The z-dependence of the density in an isothermal sheet varies as $\mathrm{sech}^2(z/2h_z)$, where $2h_z$ is the isothermal scale height. Van der Kruit & Searle (1981a, 1981b) showed that this representation applies well to surface photometry of some edge-on galaxies. However, Wainscoat, Freeman, & Hyland (1989) found that an exponential dependence of $\rho_z(z)$ provides a better description of the vertical light distribution in IC 2531. In their analysis of NGC 4314, QFG estimated the exponential scale height h_z as $(1/12)h_R$, where h_R is the radial scale length. QFG also tested the constant M/L assumption by deriving the $J-K$ color index across the disk of NGC 4314. Little color variation was found, prompting them to conclude that the constant M/L assumption was realistic, especially in the bar region.

The issue of whether to use an exponential rather than an isothermal density law in our analysis is a complex one. De Grijs (1998) has presented a new detailed study of highly inclined disk galaxies in the K' (2.1 μm) band. Since the near-infrared light is relatively insensitive to contamination by galactic dust, he has followed the vertical light distributions down to the galactic planes. He finds that such distributions are more peaked than expected for a $\mathrm{sech}(z)$ distribution but rounder than an exponential function. However, he has demonstrated that it is possible for all the galaxies in his sample to have intrinsically exponential vertical surface brightness distributions. Elmegreen & Block (1999) have demonstrated that disks that are exponential in both the radial and perpendicular directions give excellent fits to the profoundly asymmetric red-to-blue $V-K$ color profiles found along the minor axes of many spiral galaxies.

The scale heights of our largely face-on galaxies are not known; thus we can only assume values in our analysis. As noted by Freeman (1996), some bars are thicker than their disks, while others are probably about the same thickness. He notes that the bar/bulge of our Galaxy has a similar exponential scale height to the old disk. The average blue absolute magnitude of the galaxies in our sample is -20.5 ± 0.8, comparable to the Milky Way (de Vaucouleurs & Pence 1978). Therefore, for our *preliminary* analysis, we adopt, for all of our sample galaxies, $h_z = 325$ pc, which is the exponential scale height of our Galaxy (Gilmore & Reid 1983). Not all galaxies do have the same exponential scale height: the study by de Grijs (1998) indicates that late-type galaxies on average have a thinner disk than earlier type systems. To account for possible variations in scale height based on morphological type and for the possibility that some bars are thicker than their disks, we have made separate potential runs for $h_z = 225$ and 425 pc. In the future, it should be possible to improve our judgment of h_z by scaling from values of the radial scale length, as done by QFG. However, from de Grijs's work, the ratio h_R/h_z has a rather large scatter, ranging from 4 to 12 over the type range Sb to Sd and from 2.5 to 7 at type Sb alone.

Many of the galaxies in our sample retain their bar strength class values irrespective of scale height variations from 225 to 425 pc. When a galaxy does move from one bar strength to the next, the effect of decreasing the scale height is to increase the bar strength; increasing the scale height leads to a decrease in the bar strength. These effects were also noted by QFG in their study of NGC 4314 and by Salo et al. (1999) in their study of IC 4214. In our analysis, an uncertainty of ± 100 pc in h_z produces an average uncertainty of $\mp 13\%$ in bar strength.

5. CALCULATING THE BAR STRENGTH

Our procedure for calculating the bar strength involved several steps: (1) deprojection of a sky-subtracted H- or K-band image, using position angles and isophotal axis ratios from the Third Reference Catalogue of Bright Galaxies (de Vaucouleurs et al. 1991, hereafter RC3), except for the ringed galaxies NGC 1326, 1433, 3054, 3081, 6300, ESO 566−24, and ESO 565−11, where the deprojections are based on deep photometric and optical or H I kinematic studies (Buta 1987; Ryder et al. 1996; Buta et al. 1998; Buta et al. 2001; Purcell 1998); (2) expansion or contraction of the array to dimensions of 2^n, as required by the QFG fast Fourier transform analysis; (3) calculation of the potential with an arbitrary mass-to-light ratio of 1.00, a scale height of 225, 325, or 425 pc, and a distance from Tully (1988) or (for galaxies not in this catalog) from the linear Virgocentric flow model (Aaronson et al. 1982) and a Hubble constant of 75 km s^{-1} Mpc^{-1}; (4) derivation of the $m = 0$, or axisymmetric, part of the derived potential; (5) calculation of the mean axisymmetric radial ($\langle F_R \rangle$) and tangential (F_T) force fields; and (6) computation of the ratio map,

$$Q_T(i, j) = \frac{F_T(i, j)}{\langle F_R(i, j) \rangle} . \quad (2)$$

Note that the distance is needed only because we are assuming scale heights in parsecs. If we could infer h_z as a specific fraction of the radial scale length h_R, then no distance would be required. Also, the analysis is independent of the assumed (constant) value of the mass-to-light ratio because we are computing a force ratio. The actual force fields would scale the same way with the mass-to-light ratio.

The ratio map is our principal tool for estimating the bar strength. Figure 1 (*row 1*, *left*) shows a typical ratio map for a strongly barred galaxy, NGC 1433. The map shows four well-defined regions where the ratio reaches a maximum or minimum around or near the ends of the bar. This pattern is the *characteristic signature* of a bar. Depending on quadrant relative to the bar, these regions can be negative or positive because the sign of the tangential force changes from quadrant to quadrant (see Fig. 1, *row 1*, *middle*). The absolute values of the ratio at these points represent the maxima of Q_T in the Combes & Sanders (1981) formulation. To locate the maxima automatically, we analyze azimuthal profiles (5° steps) of Q as a function of radius and then derive Q_T at each radius. Then we derive the value and location of $Q_T^{\max}$ in each quadrant. Let Q_{bi} be the value of $Q_T^{\max}$ in quadrant *i*. Then we define the bar strength as

$$Q_b = \sum_{i=1}^{4} Q_{bi}/4 . \quad (3)$$

We analyze Q_b by quadrant because few galaxies are so symmetric that Q_T reaches its maximum at the same radius and value in all quadrants. For example, the presence of a strong spiral can make the values of Q_b somewhat different in the trailing quadrants of the bar compared to the leading quadrants, or some asymmetry in the bar itself can make the regions unequal. We use the mean error in Q_b as a measure of how well the different quadrants agreed in bar strength.

TABLE 1

BAR STRENGTH CLASSES

Class	Range in Q_b
0......	<0.05
1......	0.05–0.149
2......	0.15–0.249
3......	0.25–0.349
4......	0.35–0.449
5......	0.45–0.549
6......	0.55–0.649

Table 1 defines the bar strength classes that we base on the measured values of Q_b. Except for class 0, each class spans a range of 0.1 centered on a unit value. Thus, bar class 1 includes galaxies having $Q_b = 0.1 \pm 0.05$, bar class 2 includes galaxies having $Q_b = 0.2 \pm 0.05$, etc. With these definitions, class 0 involves a narrower range of Q_b, since Q_b cannot be negative as defined.

Table 2 lists the bar strengths so derived for a small sample of representative galaxies covering spiral and ring morphologies and over a range of Hubble types. The parameter listed as the "family" in Table 2 is from de Vaucouleurs (1963) for all galaxies in the table except IC 4290, ESO 565−11, ESO 566−24, and Maffei 2. The optical bar classifications for IC 4290 and ESO 566−24 are from Buta et al. (1998), that for ESO 565−11 is from Buta, Purcell, & Crocker (1995), and that for Maffei 2 is from Buta & McCall (1999). Using the code in Table 1, each galaxy in Table 2 was assigned to its appropriate bar strength class. The strongest bars that we find reach bar class 6, where the maximum tangential force reaches about 60% of the mean radial force. Figure 2 shows how well Q_b correlates with the de Vaucouleurs family parameter in the sample of Table 2. This shows that the threshold for calling a galaxy "SB" seems to be bar class 2. Apparently, bars become obvious at this strength and the Hubble–de Vaucouleurs classification can make no further discrimination on bar strength beyond this threshold, so that "SB" also includes galaxies up to bar

TABLE 2

BAR STRENGTHS FOR 36 GALAXIES

Galaxy	Family[a]	Q_b	Bar Class	DP Type	Galaxy	Family[a]	Q_b	Bar Class	DP Type
N0309.......	SAB	0.11 ± 0.02	1	H2β1	N4548........	SB	0.44 ± 0.03	4	H2α4
N0521.......	SB	0.18 ± 0.03	2	H2α:2	N4622........	SA	0.01 ± 0.01	0	H1α0
N0718.......	SAB	0.15 ± 0.02	2	H2β2	N4653........	S<u>A</u>B	0.04 ± 0.01	0	H2β0
N1300.......	SB	0.42 ± 0.06	4	H2α4	N4902........	SB	0.29 ± 0.04	3	H2α3
N1326.......	SB	0.16 ± 0.02	2	H2α2	N5236........	SAB	0.19 ± 0.04	2	H2α2
N1365.......	SB	0.46 ± 0.07	5	H2γ5	N5371........	S<u>A</u>B	0.19 ± 0.02	2	H2γ2
N1433.......	SB	0.38 ± 0.05	4	H2α4	N5457........	SAB	0.12 ± 0.01	1	H2α1
N1637.......	SAB	0.09 ± 0.03	1	H1γ1	N5905........	SB	0.43 ± 0.05	4	H2γ4
N2543.......	SB	0.28 ± 0.05	3	H2β3	N5921........	SB	0.38 ± 0.04	4	H2γ4
N2857.......	SA	0.09 ± 0.02	1	H2α1	N6300........	SB	0.17 ± 0.03	2	H2β2
N2997[b]......	SAB	0.06 ± 0.02	(0)	H2β0	N6782........	SAB	0.19 ± 0.02	2	H2α2
N3054.......	SAB	0.17 ± 0.02	2	H2α2	N7083[c].......	SA	0.06 ± 0.01	(0)	H2γ0
N3081.......	SAB	0.17 ± 0.02	2	H2α2	N7098........	SAB	0.20 ± 0.02	2	H2α2
N3346.......	SB	0.25 ± 0.06	3	H2β3	N7479........	SB	0.63 ± 0.08	6	H2γ6
N3992.......	SB	0.35 ± 0.05	4	H2α4	I4290	SB	0.56 ± 0.08	6	H2α6
N4051.......	S<u>A</u>B	0.24 ± 0.05	2	H2γ2	E565-11......	SB	0.28 ± 0.03	3	H2β3
N4321.......	SAB	0.12 ± 0.03	1	H2β1	E566-24......	SB	0.27 ± 0.04	3	H4β3
N4394.......	SB	0.22 ± 0.04	2	H2α2	Maffei 2......	SAB	0.27 ± 0.04	3	H2γ3

[a] From de Vaucouleurs 1963, except for Maffei 2, IC 4290, ESO 565−11, and ESO 566−24 (see text).
[b] No clear bar signature in ratio map; correct bar class in parentheses.
[c] Measured amplitude due to deprojection stretch; correct bar class in parentheses.

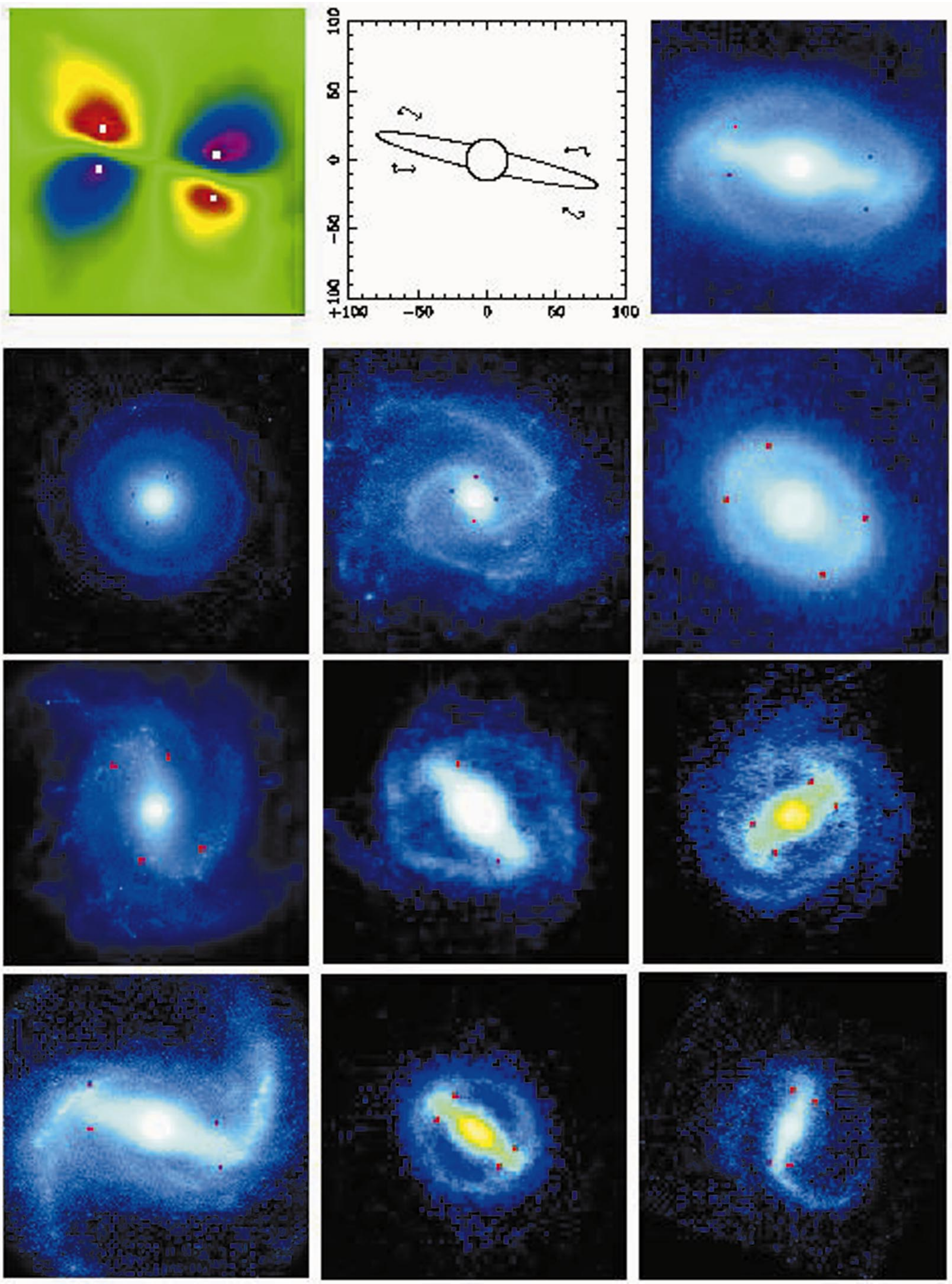

FIG. 1.—Illustration of technique: (*row 1*, *left*) ratio map for NGC 1433 (*H* band), showing maximum points in Q_b (*squares*); (*row 1*, *middle*) schematic of radial and tangential forces in NGC 1433 at the maximum points (axes in units of arcseconds for bar schematic only); (*row 1*, *right*) image of NGC 1433 with maximum points superposed (scales of these panels are all slightly different). Rows 2–4 show a sequence of galaxies of increasing Q_b: (*row 2*, *left to right*) NGC 4622 (0.01), NGC 309 (0.11), NGC 3081 (0.17); (*row 3*, *left to right*) M83 (0.19), NGC 4902 (0.29), NGC 3992 (0.35); (*row 4*, *left to right*) NGC 1365 (0.46), IC 4290 (0.56), NGC 7479 (0.63). The squares again show the locations of the maximum points.

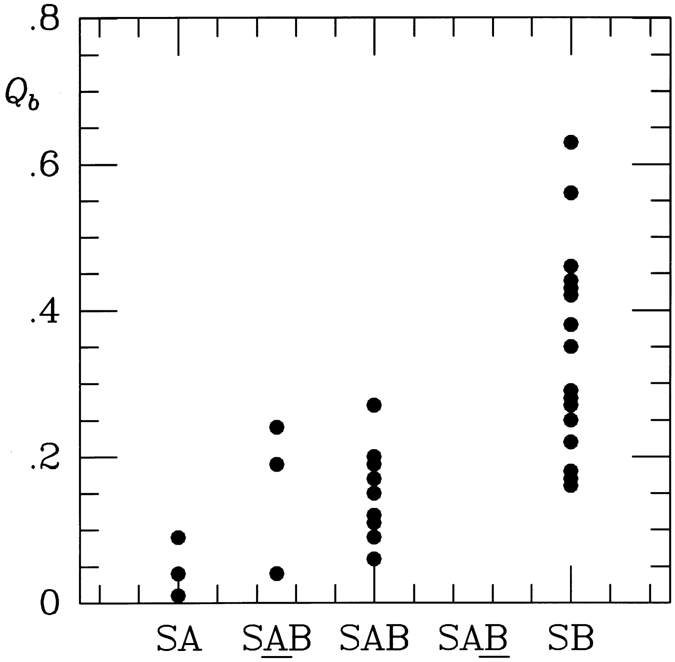

FIG. 2.—Plot of Q_b vs. de Vaucouleurs family parameter for Table 2 galaxies, where the family is taken mainly from de Vaucouleurs (1963; see text for other sources).

class 6. Galaxies classified as " SA " or " SAB " mostly range from classes 0 to 2, with the exception of Maffei 2, which is bar class 3. Maffei 2, which is a heavily reddened galaxy in the zone of avoidance, is probably the nearest massive SBbc galaxy (Spinrad et al. 1973; Hurt et al. 1993; Buta & McCall 1999).

Some of the more weakly barred galaxies in Table 2 required special treatment. For example, the measured values of Q_b for NGC 2997 and NGC 7083 indicate a bar class of 1, but we have specified their classes as (0) since either there is no clear bar signature in the ratio map or the program measured obvious deprojection stretch of the bulge.

The uncertainty attached to each value of Q_b in Table 2 includes the mean error in Q_b from the four quadrants and the uncertainty of ± 100 pc due to scale height. It excludes deprojection uncertainties, however. We consider the Q_b values in Table 2 preliminary because orientation parameters of many of the galaxies are manifestly improvable. For our analysis, we mostly used deprojected images that were already available to us, many of which were previously used for defining the dust-penetrated pitch angle classes described by Block & Puerari (1999) and Block et al. (1999). We used well-defined (kinematically and/or photometrically based) orientation parameters mainly for the ringed galaxies at this time since the deprojected images were also already available to us from earlier studies. We also used well-defined orientation parameters for Maffei 2 from Burton et al. (1996) and Buta & McCall (1999). Table 3 shows the impact of large uncertainties in the orientation parameters on Q_b for a representative barred galaxy, NGC 1300. This is a special case because the bar major axis of this galaxy is nearly along the line of nodes, making its strength very sensitive to the assumed inclination. Uncertainties of $\pm 10°$ on the inclination i and line of nodes position angle ϕ_n changes the bar strength over the bar class range 3–5.

TABLE 3

EFFECT OF UNCERTAINTY IN ORIENTATION PARAMETERS ON Q_b OF NGC 1300

i/ϕ_n	96°	106°	116°
39°...........	0.51	0.50	0.52
49°...........	0.44	0.42	0.45
59°...........	0.32	0.30	0.35

The RC3 orientation parameters of $i = 49°$ and $\phi_n = 106°$ may be compared to the values of 50° and 95°, respectively, determined from H I kinematics by England (1989). According to Table 3, NGC 1300 is still bar class 4 with England's parameters. In general, whenever the bar minor axis or major axis is nearly along the line of nodes, the effect of inclination will be most serious on Q_b.

Figure 1 (*rows 2, 3, and 4*) shows nine galaxies in our sample in a sequence of increasing Q_b, with the locations of the maximum points indicated. The mean position angle difference between the maximum points and the bar depends on the importance of higher order terms in the bar potential. For example, if the bar is a pure $m = 2$ potential, these points would lie at $\pm 45°$ to the bar axis. However, in most cases, the angle we find is less than $\pm 45°$ because of the importance of $m = 4$ and 6 terms in most real bars.

6. EVALUATION OF TECHNIQUE

Equation (1) offers a straightforward way of deriving bar strength for large numbers of galaxies in an efficient, automatic manner, subject of course to our assumptions. Studies of individual galaxies, such as NGC 7479 (Sempere, Combes, & Casoli 1995a), NGC 4321 (Sempere et al. 1995b), NGC 4314 (QFG), NGC 1300 (Lindblad & Kristen 1996), NGC 1365 (Lindblad, Lindblad, & Athanassoula 1996), NGC 4123 (Weiner 1998), and NGC 1433, 3081, and 6300 (Buta & Combes 2000) *corroborate the M/L $\sim$ constant assumption*, especially in the inner regions of galaxies. Equation (1)'s principal advantage, as we see it, is that we do not need to define the bar in any way other than to limit the analysis to the inner regions of a galaxy to avoid strong spiral structure or corner effects. It can be sensitive to deprojection uncertainties for objects like NGC 1300 (Table 3) and also in cases with roughly spherical bulges and significant inclinations, because then the artificial stretching of the bulge can produce a barlike signature. However, these are easy to identify since the bulge is stretched along the minor axis, and these are also easy to treat with bulge decomposition if there is little or no actual bar.

Excessive star formation could of course impact the computed potentials. It is well known that young red supergiants, while on the whole contributing only 3% of the total 2.2 μm flux, can be locally dominant in star-forming regions and contribute up to 33% of the flux (Rhoads 1998). We tested the impact of star formation in M100 by removing the obvious star-forming regions in the arms and bar in a K-band image, assuming that their mass-to-light ratios are much less than that of the old disk. The removal of these objects had little impact on the estimated bar strength, and the bar class was unchanged.

Q_b does not measure the shape of an *isolated* bar: it also accounts for the disk in which the bar is embedded. A comparison between our bar classes and the bar ellipticity classes of Martin (1995) shows that ellipticity class 7 (one of the strongest classes in Martin's sample) can have a bar strength class from 2 (e.g., M83) to 6 (e.g., NGC 7479), while an ellipticity class 4 galaxy can be bar strength class 0 (e.g., NGC 4653). Another example of an optically strong ellipticity bar class 7 galaxy but with a nondiscernible bar gravitational potential is NGC 4395 (J. Knapen 2000, private communication).

Q_b correlates better with the relative bar fraction, $L(\text{bar})/L(R < R_{25})$, of Elmegreen & Elmegreen (1985), although we have only three galaxies in common. NGC 1300, 3992, and 7479 have relative bar luminosities of 9.2%, 3.7%, and 20%, respectively. These same galaxies (for our adopted orientation parameters) have $Q_b = 0.42$, 0.35, and 0.63, respectively. Both Martin's and the Elmegreens' results are based on B or I images. Our sample does not overlap with the sample of Seigar & James (1998), and we cannot make a comparison between Q_b and bar equivalent angle at this time.

On the other hand, as we have noted, Q_b can be (but is not always) sensitive to the scale height, *values of which are assumed in this preliminary study*. We find that bar class is significantly sensitive to h_z only for the strongest bars; however, even in those cases the uncertainty will usually be less than 1 bar class.

7. IMPACT OF BULGE SHAPE

Our tabulated values of Q_b have ignored the shape of the bulge. In each case, the bulge has been assumed to be as flat as the disk, and only in a few cases have we treated the bulge as less flattened than the disk in order to eliminate deprojection stretch. The assumption of a highly flattened bulge is probably valid for some galaxies, such as for barred spirals with triaxial bulges (Kormendy 1982, 1993). However, in many galaxies the bulge is a much less flattened component, and even for a face-on galaxy, this could impact our bar strength estimates. If the light distribution of a spherical bulge is transformed into a potential assuming it is a thin disk, then the axisymmetric radial forces derived will be too large, especially in the inner regions. To evaluate this, we modeled the bulge of one of our galaxies, NGC 1433, whose bulge can be interpreted in terms of a highly flattened triaxial inner section and a more spherical outer section (Buta et al. 2001). The apparently round part of the bulge of NGC 1433 includes 27% of the total H-band luminosity and can be modeled as a double exponential with scale lengths of $2''$ and $11''$, both much less than the $80''$ radius of the bar. Using a program that derives forces from the light distribution by modeling the density in terms of spheroids of different flattenings (A. Kalnajs 1986, private communication), we find that our analysis overestimates the radial forces in NGC 1433 mainly for radii less than $5''$, where the error can reach a factor of 2. At the radius of the bar, the effect of the bulge shape is likely to be negligible. This may not be true in every case, and we will consider the influence of bulge shape in individual cases in more detail in a separate study. However, we note that it would be incorrect to measure bar strength only on bulge-subtracted images because the bulge contributes to the axisymmetric background regardless of its shape and Q_b should measure the strength of the bar relative to all axisymmetric luminous components.

8. A DUST-PENETRATED QUANTITATIVE CLASSIFICATION OF SPIRAL GALAXIES

The Hubble classification of galaxies is based on their optical appearance. As one moves from early- to late-type spirals, both unbarred and barred, the appearance will be dominated more and more by the young Population I component of gas and dust. However, the gaseous Population I component may only constitute 5% of the dynamical mass of a galaxy (Frogel et al. 1996).

The Hubble classification does not constrain the *dynamical mass distribution*, as corroborated by Burstein & Rubin (1985), Block (1996), and Block et al. (1999). Galaxies with bulge/disk ratios differing by a factor of 40 can have rotation curves of very similar shape; galaxies of Hubble type a, for example, may belong to any one of three different mass classes (Burstein & Rubin 1985). A late-type galaxy such as NGC 309 (optical type c) may coexist with an early type a evolved disk morphology (Block & Wainscoat 1991). The decoupling between gaseous and stellar disks can be profound, as reviewed by Block et al. (1999).

A classification scheme of spiral galaxies in the near-infrared was recently proposed by Block & Puerari (1999). The main classification parameter is the dominant Fourier harmonic in the spiral arms. In this classification, a ubiquity of low-order ($m = 1$, 2) Fourier modes for both normal and barred galaxies is found in the near-infrared regime, consistent with the modal theory of spiral structure (Bertin & Lin 1996; Block et al. 1999). Galaxies with a dominant Fourier $m = 1$ mode are L (lopsided), while galaxies principally showing an $m = 2$ harmonic are E (evensided). For simplicity, of course, any harmonic class can simply be denoted by Hm, where lopsided and evensided galaxies carry the H1 and H2 designations, respectively. Block et al. (1999) bring attention to those rarer galaxies with higher order–dominant harmonics (e.g., NGC 5054, $m = 3$, and ESO $566-24$, $m = 4$), which are assigned to harmonic classes H3 and H4, respectively.

Within these dust-penetrated harmonic classes, galaxies are binned into three subclasses based on the pitch angle of the spiral arms, robustly determined from Fourier spectra. Evolved stellar disks with tightly wound spiral arms characterized by near-infrared pitch angles of $\sim 10°$ are binned into the α class; the β class is an intermediate group, with near-infrared pitch angles of $\sim 25°$, while open stellar arms with pitch angles of $\sim 40°$ define the γ class.

These α, β, and γ classes are inextricably related to the rate of shear A/ω in the stellar disk. Here A is the first Oort constant and ω is the angular velocity. Falling rotation curves generally give rise to the α class, while rising rotation curves give rise to the γ class. For a complete discussion, see Block et al. (1999). When imaged in the near-infrared, a Hubble or de Vaucouleurs early type b galaxy may belong to class α, β, or γ; likewise for the other optical Hubble bins. Hubble type and dynamical mass distributions are not correlated (Burstein & Rubin 1985).

In this paper, we propose to simply add the bar strength derived from the inferred gravitational force fields to the shear-related pitch angle classes of Block & Puerari (1999) in order to define a more complete dust-penetrated classification system. Class 0 spirals have no bar or oval; our strongest bars are class 6. Figure 3 shows a quantitative three-pronged tuning fork for the near-infrared images of nine spiral galaxies that illustrate the full dust-penetrated

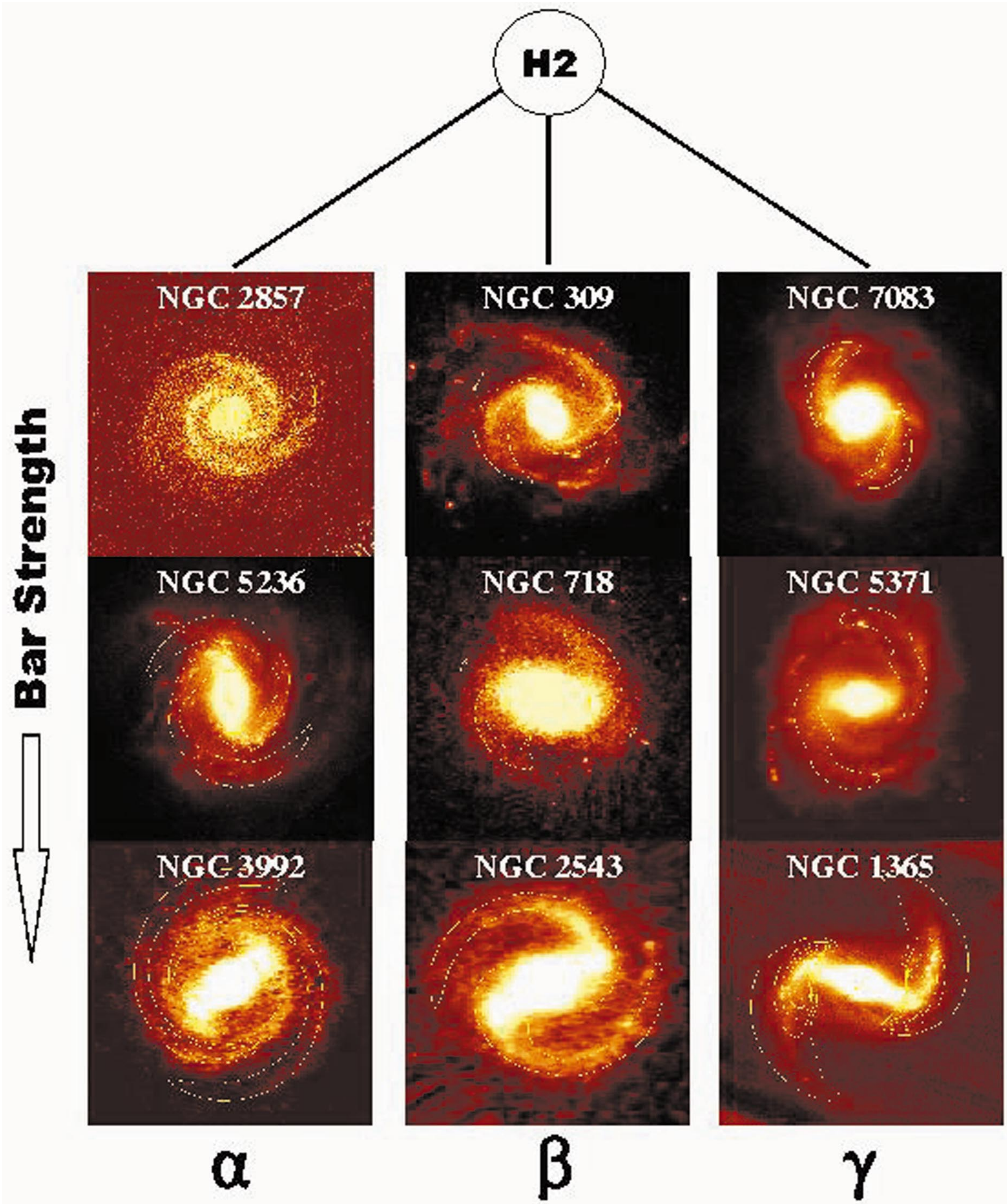

FIG. 3.—Quantitative fork for $z \sim 0$ spiral galaxies in their near-infrared dust-penetrated regime. Galaxies are binned according to three quantitative criteria: Hm, where m is the dominant Fourier harmonic (illustrated here is the two-armed H2 family); the pitch angle families α, β, or γ determined from the Fourier spectra; and the bar strength, derived from the gravitational torque (not ellipticity) of the bar. Early type b spirals (NGC 3992, NGC 2543, NGC 7083, NGC 5371, and NGC 1365) are distributed within all three families (α, β, and γ). Hubble type and dust-penetrated class are uncorrelated.

classification system for the H2 class. The images are from Block et al. (1999) and are overlaid with the contours of the main harmonic, $m = 2$.

For example, it is proposed that NGC 5236 (M83; illustrated in Fig. 3) bears the quantitative classification H2α2, implying that the bar class is 2, that the galaxy has tightly wound type α arms in the dust-penetrated regime, and that there is an evensided two-armed spiral in its evolved stellar disk. The pitch angles of the spiral arms in barred galaxies of the same Hubble type span the entire α–γ range; for example, NGC 3992 and NGC 1365 (both Hubble type b) carry the full designation H2α4 and H2γ5, respectively.

The tuning fork in Figure 3 may serve as a $z \sim 0$ template when galaxies at $z \sim 0.5$–1 are imaged in their rest-frame K dust-penetrated 2 μm regime. It is not a confirmed observational fact that the morphology of galaxies in the Hubble Deep Fields are very different in the past than in the present (R. I. Thompson 2000, private communication) when the effects of redshift and surface brightness dimming are fully accounted for (Ellis 1997; Takamiya 1999).

9. CONCLUSIONS

We have outlined the derivation of a fully quantitative bar strength class for spiral galaxies, based on the maximum value of the amplitude of the tangential force to the mean radial force. Although the method is still based on light fluxes, since we use images to infer gravitational potentials, it provides a more direct handle on bar strength than any other light-based methods so far applied. Regardless of what the bar may visually look like, the ratio map will show a pattern of four maxima/minima that can be isolated fairly automatically to give a robust measure of bar strength. The method is thus free from uncertainties connected with defining bars or with full bulge/disk decompositions. It can be applied quickly and efficiently to many galaxies, and only in some cases is it necessary to give special treatment to the bulge if it suffers too much deprojection stretch. Bulge shape, dark matter, and star formation have little impact on the bar strength class for our sample galaxies. The most important effects are vertical scale height and, for highly inclined galaxies, deprojection uncertainties.

The method has much room for refinement. For example, bulges can be decomposed to eliminate deprojection stretch and their influence on the ratio maps more accurately accounted for. Improved orientation parameters can be used or derived for galaxies as data become available. Appropriate vertical scale heights could be inferred more reliably from detailed near-infrared surface photometry and the type dependence of h_R/h_z. The validity of the constant M/L assumption could be tested by measuring $J-K$ color distributions. Finally, deprojection uncertainties go beyond simple bulge deprojection stretch to the fundamental uncertainty of deprojecting any galaxy, even if a bulge is not present. All of these are issues that will be considered in a more detailed forthcoming study.

The addition of our bar strength parameter to the dust-penetrated classification scheme of Block et al. (1999) now gives a full dynamical appreciation of the range of evolved stellar disks with bars (Fig. 3).

We thank A. Quillen, F. Combes, A. Kalnajs, and S. M. G. Hughes for programs that were used in this study. We also thank A. Quillen, F. Combes, B. Elmegreen, K. Freeman, P. van der Kruit, A. Kalnajs, R. de Grijs, R. I. Thompson, and especially the (anonymous) referee for helpful and timely advice and comments that improved this study. D. Elmegreen, I. Puerari, P. Grosbøl, J. Knapen, K. C. Freeman, O. K. Park, and T. Jarrett very graciously loaned us some images that we used to test the bar strength method. We thank D. A. Crocker for her assistance in producing the tuning fork diagram in Figure 3. We gratefully acknowledge the support of the Anglo-American Chairman's Fund, which also made the visit to South Africa of one of us (R. B.) possible. We are indebted to CEO Mrs. M. Keeton and the Board of Trustees.

REFERENCES

Aaronson, M., Huchra, J., Mould, J., Schechter, P., & Tully, R. B. 1982, ApJ, 258, 64
Abraham, R., & Merrifield, M. R. 2000, AJ, 120, 2835
Abraham, R., Merrifield, M. R., Ellis, R. S., Tanvir, N. R., & Brinchmann, J. 1999, MNRAS, 308, 569
Aguerri, J. A. L. 1999, A&A, 351, 43
Athanassoula, E. 1992, MNRAS, 259, 328
Bertin, G., & Lin, C. C. 1996, Spiral Structure in Galaxies: A Density Wave Theory (Cambridge: MIT Press)
Binney, J., & Tremaine, S. 1987, Galactic Dynamics (Princeton: Princeton Univ. Press)
Block, D. L. 1996, in New Extragalactic Perspectives in the New South Africa, ed. D. L. Block & J. M. Greenberg (Dordrecht: Kluwer), 1
Block, D. L., Bertin, G., Stockton, A., Grosbøl, P., Moorwood, A. F. M., & Peletier, R. F. 1994, A&A, 288, 365
Block, D. L., & Puerari, I. 1999, A&A, 342, 627
Block, D. L., Puerari, I., Frogel, J. A., Eskridge, P. B., Stockton, A., & Fuchs, B. 1999, Ap&SS, 269, 5
Block, D. L., & Wainscoat, R.J. 1991, Nature, 353, 48
Burstein, D., & Rubin, V. 1985, ApJ, 297, 423
Burton, W. B., Verheijen, M. A. W., Kraan-Korteweg, R. C., & Henning, P. A. 1996, A&A, 309, 687
Buta, R. 1986, ApJS, 61, 609
———. 1987, ApJS, 64, 383
———. 1995, ApJS, 96, 39
Buta, R., Alpert, A. J., Cobb, M. L., Crocker, D. A., & Purcell, G. B. 1998, AJ, 116, 1142
Buta, R., & Combes, F. 1996, Fundam. Cosmic Phys., 17, 95
———. 2000, in ASP Conf. Ser. 197, Dynamics of Galaxies: From the Early Universe to the Present, ed. F. Combes, G. A. Mamon, & V. Charmandaris (San Francisco: ASP), 11
Buta, R., & McCall, M. L. 1999, ApJS, 124, 33
Buta, R., Purcell, G. B., & Crocker, D. A. 1995, AJ, 110, 1588
Buta, R., Ryder, S. D., Madsen, G., Wesson, K., Crocker, D. A., & Combes, F. 2001, AJ, 121, 225
Chapelon, S., Contini, T., & Davoust, E. 1999, A&A, 345, 81
Combes, F., & Sanders, R. H. 1981, A&A, 96, 164
Debattista, V., & Sellwood, J. A. 1998, ApJ, 493, L5
Debattista, V., & Sellwood, J. A. 2000, ApJ, 543, 704
de Grijs, R. 1998, MNRAS, 299, 595
de Vaucouleurs, G. 1955, AJ, 60, 126
———. 1959, Handbuch der Physik, 53, 275
———. 1963, ApJS, 8, 31
de Vaucouleurs, G., & de Vaucouleurs, A. 1959, PASP, 71, 83
de Vaucouleurs, G., et al. 1991, Third Reference Catalogue of Bright Galaxies (New York: Springer) (RC3)
de Vaucouleurs, G., & Pence, W. D. 1978, AJ, 83, 1163
Ellis, R. 1997, ARA&A, 35, 389
Elmegreen, B. G., & Block, D. L. 1999, MNRAS, 303, 133
Elmegreen, D. M., Chromey, F. R., Bissell, B. A., & Corrado, K. 1999, AJ, 118, 2618
Elmegreen, B. G., & Elmegreen, D. M. 1985, ApJ, 288, 438
England, M. N. 1989, ApJ, 337, 191
Eskridge, P. B., & Frogel, J. A. 1999, Ap&SS, 269, 427
Eskridge, P. B., et al. 2000, AJ, 119, 536
Freeman, K. C. 1989, in Gérard and Antoinette de Vaucouleurs: A Life for Astronomy, ed. M. Cappacioli & H. G. Corwin, Jr. (Singapore: World Scientific), 85
———. 1992, in Physics of Nearby Galaxies: Nature or Nurture? ed. T. X. Thuan, C. Balkowski, & J. Tran Thanh Van (Gif-sur-Yvette: Editions Frontiere), 201
———. 1996, in ASP Conf. Ser. 91, Barred Galaxies, ed. R. Buta, D. A. Crocker, & B. G. Elmegreen (San Francisco: ASP), 1
Frogel, J. A., Quillen, A. C., & Pogge, R. W. 1996, in New Extragalactic Perspectives in the New South Africa, ed. D. L. Block & J. M. Greenberg (Dordrecht: Kluwer), 65
Gilmore, G., & Reid, N. 1983, MNRAS, 202, 1025
Hubble, E. 1926, ApJ, 64, 321
Hurt, R. L., Merrill, K. M., Gatley, I., & Turner, J. L. 1993, AJ, 105, 121
Jarrett, T. H. 2000, PASP, 112, 1008
Kormendy, J. 1979, ApJ, 227, 714
———. 1982, ApJ, 257, 75
———. 1993, in IAU Symp. 153, Galactic Bulges, ed. H. Dejonghe & H. J. Habing (Dordrecht: Kluwer), 209
Lindblad, P. A. B., & Kristen, H. 1996, A&A, 313, 733
Lindblad, P. A. B., Lindblad, P. O., & Athanassoula, E. 1996, A&A, 313, 65

Martin, P. 1995, AJ, 109, 2428
Martin, P., & Friedli, D. F. 1997, A&A, 326, 449
Martin, P., & Roy, J. R. 1994, ApJ, 424, 599
Mathewson, D. S., Ford, V. L., & Buchhorn, M. 1992, ApJS, 81, 413
Ohta, K., Masaru, H., & Wakamatsu, K. 1990, ApJ, 357, 71
Persic, M., Salucci, P., & Stel, F. 1996, MNRAS, 281, 27
Pfenniger, D., Martinet, L., & Combes, F. 1996, in New Extragalactic Perspectives in the New South Africa, ed. D. L. Block & J. M. Greenberg (Dordrecht: Kluwer), 291
Purcell, G. B. 1998, Ph.D. thesis, Univ. Alabama
Quillen, A. C. 1996, in ASP Conf. Ser. 91, Barred Galaxies, ed. R. Buta, D. A. Crocker, & B. G. Elmegreen (San Francisco: ASP), 390
Quillen, A. C., Frogel, J. A., & González, R. A. 1994, ApJ, 437, 162 (QFG)
Rhoads, J. E. 1998, AJ, 115, 472
Rozas, M., Knapen, J. H., & Beckman, J. E. 1998, MNRAS, 301, 631
Ryder, S. D., Buta, R., Toledo, H., Shukla, H., Staveley-Smith, L., & Walsh, W. 1996, ApJ, 460, 665
Salo, H., Rautiainen, P., Buta, R., Purcell, G. B., Cobb, M. L., Crocker, D. A., & Laurikainen, E. 1999, AJ, 117, 792
Sandage, A. 1961, The Hubble Atlas of Galaxies (Publ. 618; Washington, DC: Carnegie Institution)
Sandage, A., & Bedke, J. 1994, The Carnegie Atlas of Galaxies (Publ. 638; Washington, DC: Carnegie Institution)
Seigar, M. S., & James, P. A. 1998, MNRAS, 299, 672
Sellwood, J. A., & Wilkinson, A. 1993, Rep. Prog. Phys., 56, 173
Sempere, M. J., Combes, F., & Casoli, F. 1995a, A&A, 299, 371
Sempere, M. J., Garcia-Burillo, S., Combes, F., & Knapen, J. H. 1995b, A&A, 296, 45
Shlosman, I., Peletier, R. F., & Knapen, J. H. 2000, ApJ, 535, L83
Spinrad, H., Bahcall, J., Becklin, E. E., Gunn, J. E., Kristian, J., Neugebauer, G., Sargent, W. L. W., & Smith, H. 1973, ApJ, 180, 351
Takamiya, M. 1999, ApJS, 122, 109
Tully, R. B. 1988, Nearby Galaxies Catalogue (Cambridge: Cambridge Univ. Press)
van der Kruit, P., & Searle, L. 1981a, A&A, 95, 105
———. 1981b, A&A, 95, 116
Wainscoat, R. J., Freeman, K. C., & Hyland, A. R. 1989, ApJ, 337, 163
Weiner, B. J. 1998, Ph.D. thesis, Rutgers Univ.